

Ground-based observations of diffuse auroral frequencies in the context of whistler mode chorus

M. Samara¹ and R. G. Michell¹

Received 30 September 2009; revised 12 April 2010; accepted 6 May 2010; published 2 September 2010.

[1] We present a case study of an active auroral event containing diffuse auroral structures. These data were collected on 04 February 2009 during a ground-based observational campaign at Poker Flat, Alaska ($L \sim 6$), from January through April 2009. They were used to extract the frequencies of pulsating auroral structures that lasted many hours after substorm breakup. There are two main frequency ranges reported, coincident with the spatial resolution capabilities of the two different fields of view of the optical imagers used. The all-sky imager clearly revealed the pulsations of the large patches, ranging from approximately 50 to 500 mHz. The narrowfield imager measured the pulsations within the finer structure to be in the range of 0.5 to 15 Hz. Both observations are consistent with the frequencies expected from theoretical, modeling and observational work on whistler mode chorus and ECH waves. In particular, the repetition frequencies observed in the visual aurora closely match the observed repetition rate of discrete chorus elements previously described in the literature. There are three significant additional insights gained through these data. The frequency of the pulsations correlates to the intensity of the aurora, with the brighter aurora containing higher frequencies. The scale size of the structures relates to the frequency of the pulsations, with the smaller structures occurring with higher frequency pulsations. The intensity profile of the pulsating structures is not symmetric, with the intensity increasing at a slower rate than it decreases.

Citation: Samara, M., and R. G. Michell (2010), Ground-based observations of diffuse auroral frequencies in the context of whistler mode chorus, *J. Geophys. Res.*, *115*, A00F18, doi:10.1029/2009JA014852.

1. Introduction and Background

[2] The temporal variations of diffuse auroral structures, originating from pitch angle scattered magnetospheric electrons, can be used to study the wave activity causing the scattering. These periodic variations in auroral luminosity reflect the modulations of this wave activity. This article investigates the connection between discrete chorus elements and the temporal frequencies observed within the diffuse aurora.

[3] The relationship between diffuse aurora and magnetospheric plasma waves was discussed most recently [Meredith *et al.*, 2009; Ni *et al.*, 2008], in the context of in situ observations of the waves. The two main wave modes that can resonate with magnetospheric electrons in the 100 eV to few keV energy range are electron cyclotron harmonic (ECH) waves and chorus waves [Meredith *et al.*, 2009]. Electrons in this range (100 eV to few keV) contain sufficient energy to produce visible aurora. Observations from the 1970s [Kennel *et al.*, 1970; Lyons, 1974] using OGO-5 data revealed that ECH waves had amplitudes large enough to scatter keV particles. However, observations from the 1980s, using GEOS 2 satellite data, found that most of the

time the ECH waves did not contain enough energy to scatter these electrons, and were therefore not a significant source of scattering for the diffuse auroral electrons [Belmont *et al.*, 1983].

[4] It has been suggested by Peticolas *et al.* [2002], using the FAST satellite and airborne imagers, that ECH waves are generally responsible for scattering less than 2 keV plasma sheet electrons, and that upper band whistler mode chorus is responsible for scattering the higher energy (≥ 2 keV) plasma sheet electrons into the loss cone. It is these chorus waves that are thought to be responsible for scattering the electrons that produce the diffuse auroral emissions that are observed using ground-based imagers. Sergienko *et al.* [2008], using FAST and ground-based imagers, found that ECH waves were responsible for scattering the lower energy electrons (3–4 keV) that produce the structureless background auroral luminosity, while whistler mode chorus was responsible for scattering the ≥ 4 keV electrons that cause the fine structures visible within the diffuse aurora. This is consistent with the observations of Peticolas *et al.* [2002], where they concluded that black aurora was caused by a localized suppression of the chorus waves.

[5] Chorus waves in the few kHz range are typically observed to occur in groups of successive elements, each with a rising frequency [Trakhtengerts, 1999]. There have been many observations of chorus elements reported in the

¹Southwest Research Institute, San Antonio, Texas, USA.

literature with ranges of element duration, spacing and grouping. For example, *Skoug et al.* [1996] reported chorus element durations of around 0.5 s, using rocket data. In addition, the four Cluster II spacecraft, with the capability of making high resolution observations of chorus waves, have provided an excellent opportunity to study the duration and repetition of discrete chorus elements in detail. *Breneman et al.* [2009] present an example of high resolution Cluster data, showing discrete chorus elements occurring in groups with element spacings of ~ 0.1 s with a few seconds between groups. Further Cluster observations of discrete chorus elements are presented by *Nunn et al.* [2009, Figures 2 and 3], where the spacing between elements ranges from 0.1 to 0.2 s and the spacing between groups is approximately 2 to 3 s. To sum up, the observational data have shown that the chorus element duration ranges from ~ 1.0 s [*Breneman et al.*, 2009] down to ~ 0.1 s [*Nunn et al.*, 2009]. The individual element spacings range between 0.1 and 5 s, while the grouping is typically from 1 to 10 s [*Trakhtengerts*, 1999].

[6] These observed frequencies of 1.0 to 10 Hz closely match the frequencies of ultra low frequency (ULF) waves as well as the luminosity variations associated with the pulsating auroral structures presented in this paper. It has been suggested by *Kokubun et al.* [1981] that ULF waves are caused by conductivity enhancements generated by the electron precipitation induced by chorus elements. More recent work has shown that ULF waves may be responsible for accelerating high energy electrons [*O'Brien et al.*, 2003; *Degeling et al.*, 2008] that in turn cause electron microbursts [*O'Brien et al.*, 2003]. Therefore the relative roles of ULF waves and chorus in scattering the electrons responsible for producing auroral structures is a topic of interest.

[7] Diffuse pulsating auroral structures after a substorm onset are a common phenomenon of the auroral ionosphere. For this study, one particular example, which persisted several hours after a substorm onset, was chosen for investigation of the temporal evolution of the pulsating structures. There was a range in the size, shape and frequency of the pulsating features that were observed simultaneously with several ground-based instruments. Three distinct periods were observed, each of which will be investigated. It is the purpose of the present work to quantify the pulsating frequencies and the spatial scales with which they occur, taking full advantage of these high time resolution measurements. Moreover, these temporal and spatial scales are discussed in the context of the in situ wave scattering mechanisms involving chorus elements, thus far reported in the literature. Specifically, we compare the characteristics of discrete chorus elements with the characteristics of the auroral luminosity variations within pulsating auroral structures.

2. Observations

[8] The data presented here were collected during an observational campaign at Poker Flat, Alaska ($L \sim 6$), from January through April 2009. Several imagers were operated, including an intensified white-light all-sky, and an electron multiplying CCD (EMCCD) narrowfield imager with a $14^\circ \times 14^\circ$ FOV. The latter was centered on the magnetic zenith and it was equipped with a Schott BG3 glass filter, which removes light in the range of 4500 to 7000 Å, trans-

mitting the prompt blue and near-IR emissions. The all-sky imager data, recorded at 30 frames per second, result in a spatial resolution of 600 m at 100 km altitude. The EMCCD data, recorded at 33 frames per second, result in a spatial resolution of 60 m at 100 km altitude. In addition, the Poker Flat Incoherent Scatter Radar (PFISR) was running a mode consisting of long pulses ($480 \mu\text{s}$) in five beam positions, one located along the magnetic field-aligned direction ($Az. = -154.3^\circ$, $El. = 77.5^\circ$), and one each approximately 2° to the North, South, East and West of magnetic zenith respectively. The integrated PFISR data have a time resolution of approximately 5.5 seconds.

[9] The event in this study occurred on 04 February 2009, where a substorm was followed by several hours of diffuse aurora with pulsating frequencies in the range of 0.1 to ~ 10 Hz. Figure 1 shows an overview of the electron density profiles from PFISR over the course of the night, taken from the magnetic field aligned beam position. The substorm activation can be seen near 1040 UT. This was followed by a period of decreased ionization, lasting approximately one hour. During this time period there were large (~ 10 – 50 km) pulsating auroral patches moving West to East through the all-sky images. Near 1220 UT there was a significant increase in the ionization that lasted more than one hour, during which there were both slow (0.1 Hz) and fast (5–10 Hz) pulsating auroral structures. The black vertical lines delineate the three distinct time periods to be investigated in detail.

[10] Figure 2 shows a series of all-sky images taken every 15 minutes, starting at 1030 UT, during the course of this event. North is down and East is to the right. There is a clear substorm expansion near 1045 UT, as well as a second intensification within the diffuse structures near 1230 UT, which contained simultaneous pulsating structures. Figure 3 shows a series of EMCCD narrowfield images taken at the same time as the all-sky images in Figure 2. These images are all centered on the magnetic zenith, revealing the small-scale structures present there.

[11] Several different time periods are examined, in order to quantify the temporal frequencies within the aurora and investigate their connection to in situ wave processes. Poker Flat is at an L -value of 5.7 and during active times, the MLT midnight to morning sector is expected to contain both chorus and ECH waves [*Meredith et al.*, 2009]. The actual substorm breakup occurred at ~ 1040 UT (2320 MLT), and the subsequent pulsating started at ~ 1050 UT (2330 MLT). The shape, size and frequency of the pulsating structures continued to change and evolve during the course of the event. Each of these time periods is examined in detail in the next sections: 1050–1120 UT (2330–2400 MLT), 1120–1215 UT (2400–0055 MLT), and 1220–1420 UT (0100–0300 MLT).

2.1. Time Period 1 (1050–1120 UT)

[12] Figure 4 is a keogram of the all-sky imager data from 1050 to 1120 UT, at one second cadence. It shows the large scale structure of the aurora during this time period, including the general southward motion after the substorm injection. The pulsations become more visible when the data are presented over a shorter time interval. Figure 5 shows a keogram, in the same format as Figure 4, spanning five minutes from 1110 to 1115 UT, where the ~ 10 second periodicities are clear. A fast Fourier transform (FFT), along

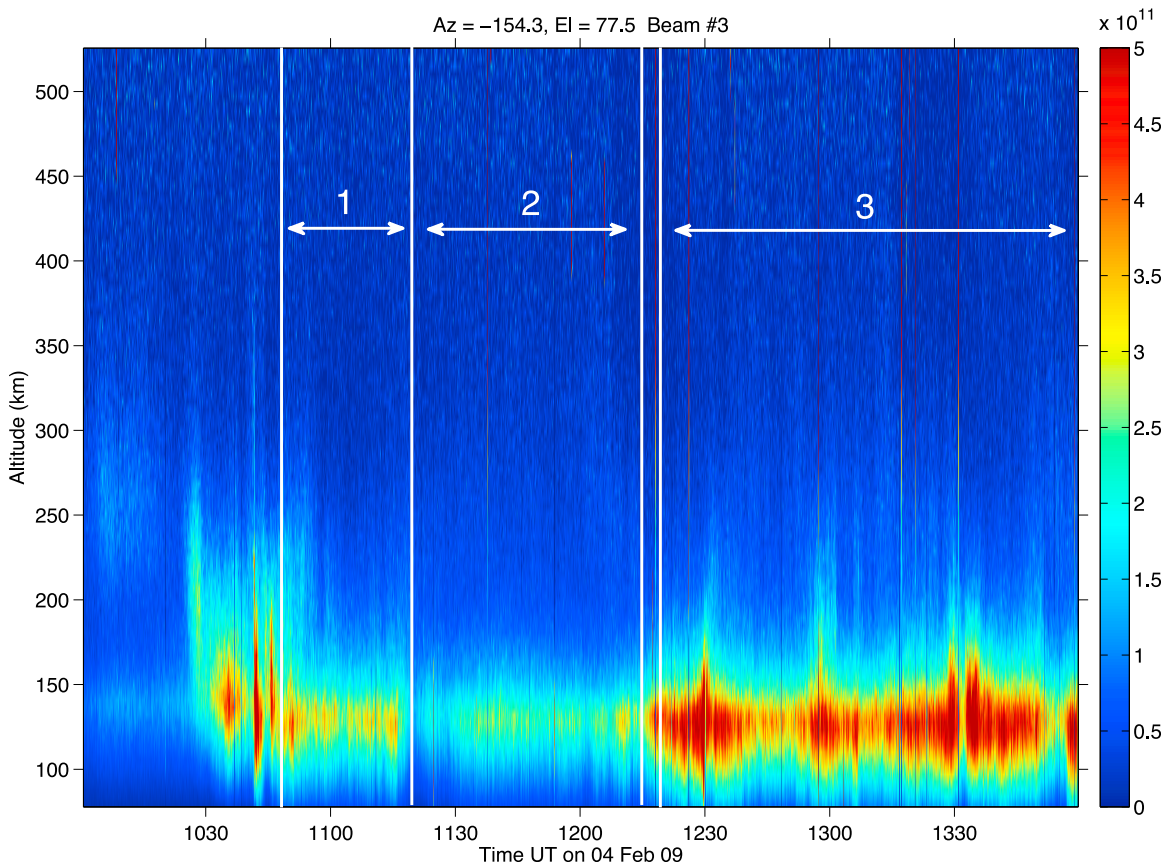


Figure 1. Electron density measured by PFISR, in m^{-3} , as a function of altitude and time for 04 February 2009, taken along the magnetic field aligned direction. The three time intervals of interest are shown.

pixel number 200 of Figure 4, which is near the magnetic zenith, was taken over the whole time interval, in order to discern the exact frequency components of the pulsations.

[13] Figure 6 (top) shows the intensity as a function of time and (bottom) the FFT of that intensity profile. These all-sky data reveal significant power at frequencies less than ~ 100 mHz, which increases toward lower frequencies. The all-sky images, a subset of which is displayed in Figure 2 at a 15 minute cadence, reveal that the low frequency pulsations occur on spatial structures of 10–50 km in size, assuming 100 km altitude.

[14] An examination of the all-sky data alone, even at 30 frames per second, does not reveal any small scale (≤ 1 km) structure or higher frequency (≥ 1 Hz) pulsations. The narrowfield imager data at 33 frames per second, show an abundance of small scale features that contain higher frequency pulsations. Figure 7 (top) shows a keogram from the EMCCD narrowfield imager, during a period of 30 seconds taken near 1110 UT (within the period covered by Figure 5). This clearly reveals the occurrence of higher frequency pulsations associated with small scale auroral structures. Figure 7 (middle and bottom) shows the intensity profile taken along the center of the keogram and the FFT of this intensity cut, respectively. There is a range of frequencies present and most of the power is contained below ~ 8 Hz, with the exception of a distinct peak near 11.5 Hz. Moreover, it is clear from Figure 7 (top) that there is a higher

frequency of ~ 3 Hz within the localized brightening occurring between 23 and 25 seconds, in addition to the lower frequency of ~ 1 Hz present throughout. This is an indication that the waves responsible for this increased scattering contain more power at higher frequencies.

2.2. Time Period 2 (1120–1215 UT)

[15] The Figure 8 keogram from 1120 to 1215 UT, shows a southward motion of the brightest region of diffuse aurora. The large scale, low frequency pulsating structures can be seen best around 1200 UT, but a shorter timescale is needed to clearly discern the pulsations. Figure 9 shows a zoom in on the keogram from 1200 to 1210 UT, where several distinct pulsating structures can be seen, as well as pulsations forming at the southern edge of the brighter auroral arc in the North.

[16] An intensity cut and FFT were taken near the magnetic zenith, to determine the pulsating frequencies within this time period. Figure 10 (top) shows the intensity, along pixel number 200 of Figure 8, as a function of time. Figure 10 (bottom) shows the FFT of that intensity profile.

[17] From Figure 10, the low frequency power contained within this period is similar to period 1, only in this case the power is mostly contained in frequencies less than 50 mHz with increasing power toward lower frequencies.

[18] The higher frequency pulsations that occur in this region are only visible with the narrowfield imager. Figure 11

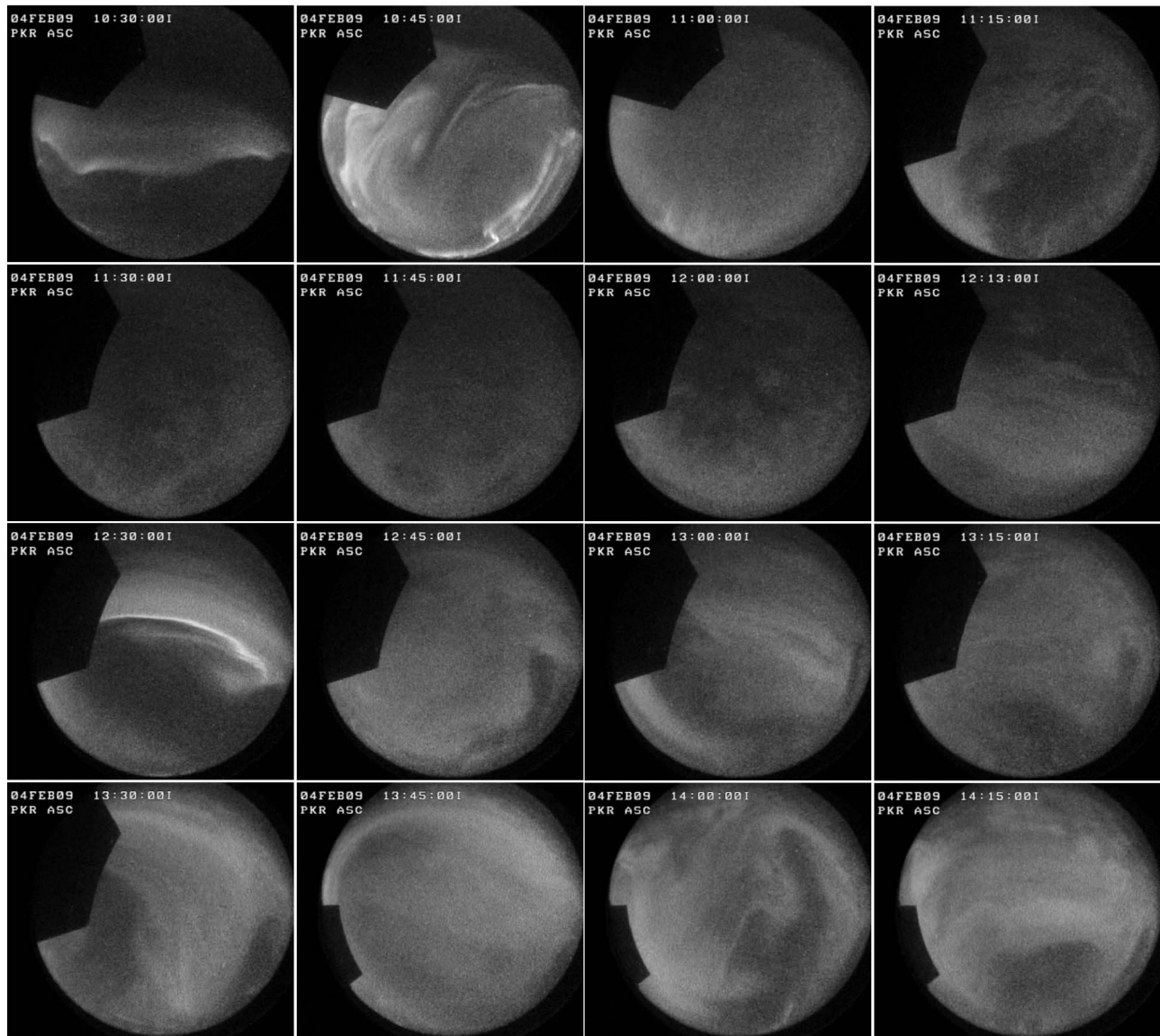


Figure 2. Series of all-sky images showing the development of this event, taken at 15 min intervals. North is down, and East is to the right in these images.

(top) is a keogram from the EMCCD narrowfield imager, covering a period of 30 seconds, taken near 1205 UT, which is within the period covered by Figure 9. This reveals the occurrence of higher frequency pulsations associated with small scale auroral structures. Figure 11 (middle and bottom) shows the intensity profile taken along the center of the keogram and the FFT of the intensity cut, respectively.

[19] Figure 11 shows a distinct 12 second periodicity (83 mHz), however there were many higher frequency pulsations occurring simultaneously. The FFT reveals that most of the power is contained in pulsations with frequencies up to 6 Hz. One thing to note about the 12 second pulsations, is that their increase in brightness is slower than their decrease. This appears to be a common feature among the many different pulsating auroral structures we have examined.

2.3. Time Period 3 (1220–1420 UT)

[20] The Figure 12 all-sky keogram from 1220 to 1420 UT, shows the large scale structure of the aurora during this time. The auroral intensity is higher and some of the pulsations are visible on this long timescale. A zoom in on an eight minute period (Figure 13), reveals clear pulsations, with periods of ~ 10 seconds, during this whole period and extending throughout the majority of the auroral structure present.

[21] Figure 14 shows an intensity cut and FFT near the magnetic zenith. Figure 14 (top) shows the intensity along pixel number 200 of Figure 12 as a function of time, and Figure 14 (bottom) shows the FFT of that intensity profile. In this case, the power again increases toward lower frequencies but it is contained within the region ≤ 150 mHz, contrary to the two previous time periods.

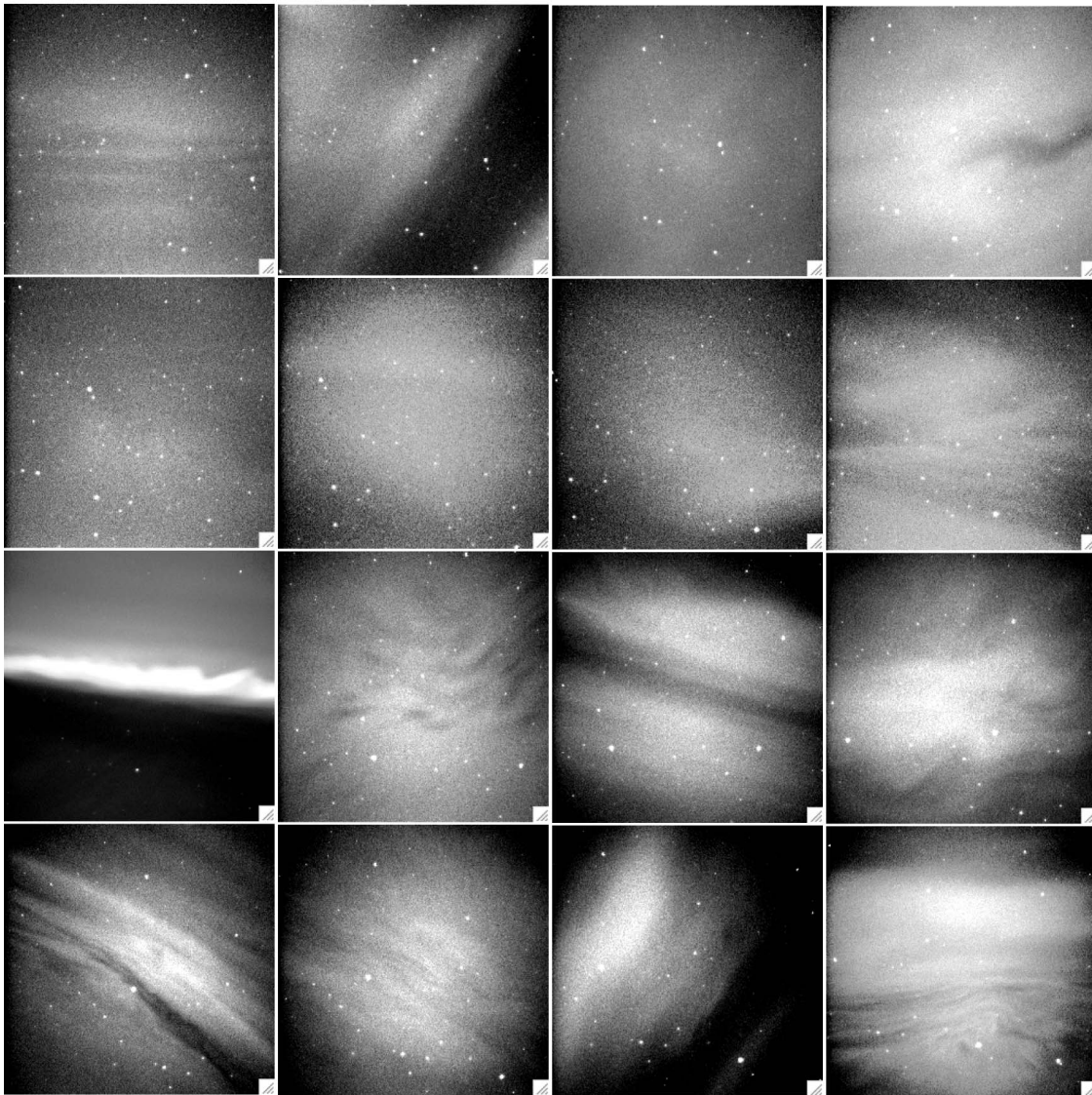


Figure 3. Series of EMCCD narrowfield images taken at the same time as the all-sky images in Figure 2. North is down, and East is to the right in these images. Each image represents approximately 25×25 km, assuming 100 km altitude.

[22] The narrowfield data for this region also reveals significant power contained within a larger range of frequencies. Figure 15 (top) shows a keogram from the EMCCD narrowfield imager, covering a period of 30 seconds, taken near 1325 UT, within the period of the keogram in Figure 13. Figure 15 (middle) is the intensity profile taken along the center of the keogram and Figure 15 (bottom) shows the FFT of the intensity cut. This example contains well defined small scale (≤ 1 km) structure with clearly visible pulsations at many different frequencies. During this time the power was contained in frequencies up to approximately 12 Hz.

3. Discussion

[23] The event examined commences with a distinct substorm onset followed by a temporally changing diffuse aurora region, therefore presenting a good case study. The temporal changes enabled different regions of the auroral

ionosphere, and thus different L-shells, to be in the magnetic zenith. The PFISR and imager data provided the method for distinguishing when each of the three temporally defined regions is in the zenith.

[24] The first period (1050–1120 UT), contains the freshly injected plasma which is observed to move to lower L-shells after the substorm, as evidenced by the southward expansion of the diffuse auroral structures. There is a lag of approximately 10 min between substorm onset and the appearance of pulsations in the zenith. ULF waves are likely generated at substorm onset, [Zolotukhina *et al.*, 2008; Liang *et al.*, 2009], but the observation of the pulsations is delayed. This may simply be due to the fact that there is a lingering energy flux of electrons from the substorm current wedge, which results in auroral luminosity (discrete aurora) bright enough to obscure the pulsations. Once this high energy flux dissipates, the pulsations become visible. This is consistent with the PFISR data in Figure 1, where the electron density

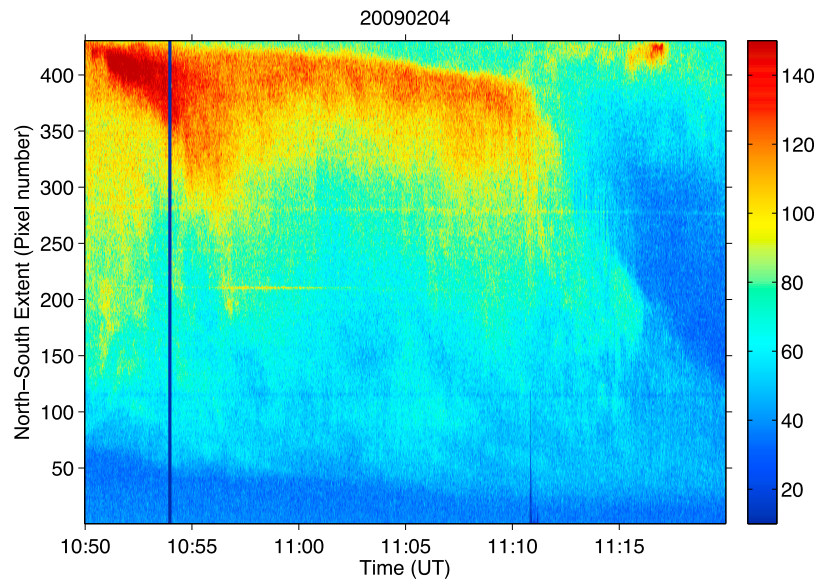


Figure 4. Keogram along the North–South direction, through the center of the all-sky image for the time period 1050–1120 UT. North is up, the horizontal lines are stars, and the dark vertical line is a data gap.

is enhanced at higher altitudes (150–250 km) until approximately 1050 UT.

[25] *Trakhtengerts* [1999] postulated that pulsating patches could result from separate ducts of enhanced cold plasma density that would remain as coherent structures and have pulsation periods of 2 to 20 s. This is consistent with a generation mechanism where a burst of chorus elements should appear in the final seconds of the optical brightening of the pulsating aurora. The pulsation observations pre-

sented here, specifically time period 2, show evidence of temporal evolution during the pulsating patch, consistent with the mechanism of *Trakhtengerts* [1999]. The intensity of the aurora is not symmetric about the pulsating patch, a common feature in the many different events examined, where the intensity increases at a slower rate than it decreases. This could be the result of the increase in frequency of the chorus bursts, until they reach a cutoff, where they no longer resonate with the plasma sheet electrons of the correct

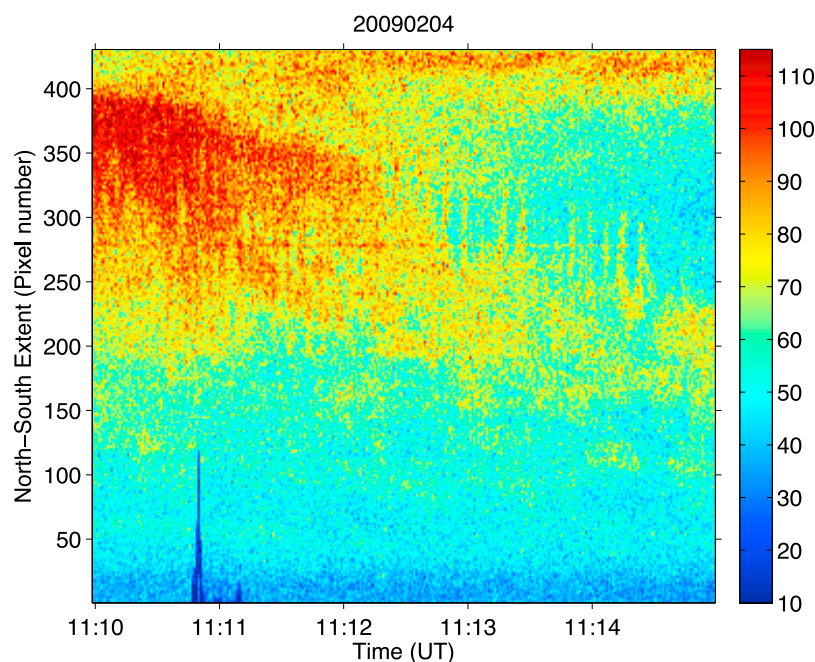


Figure 5. Five minute section (1110–1115 UT) of the keogram in Figure 4, presented in the same format.

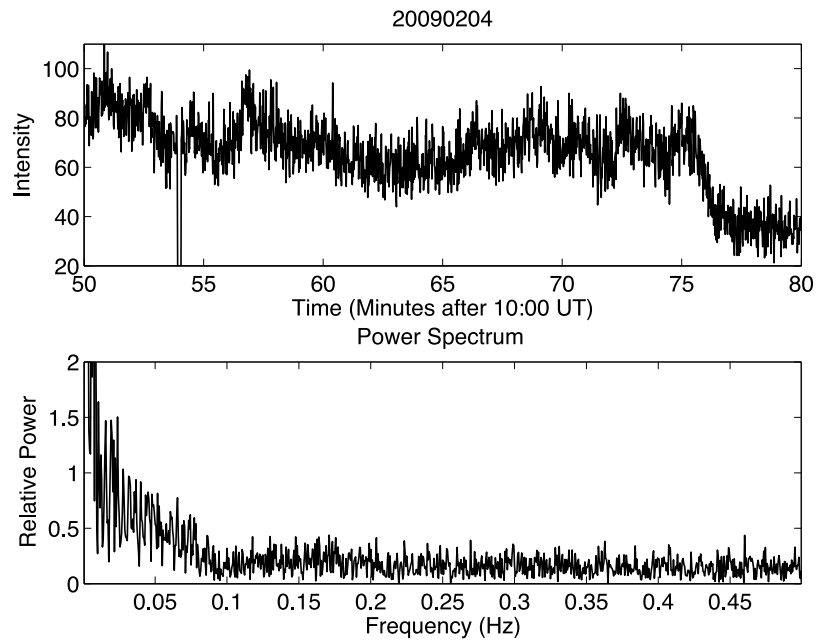


Figure 6. (top) Intensity as a function of time near the magnetic zenith (along pixel number 200 of Figure 4) from the all-sky imager data. (bottom) FFT of the intensity profile.

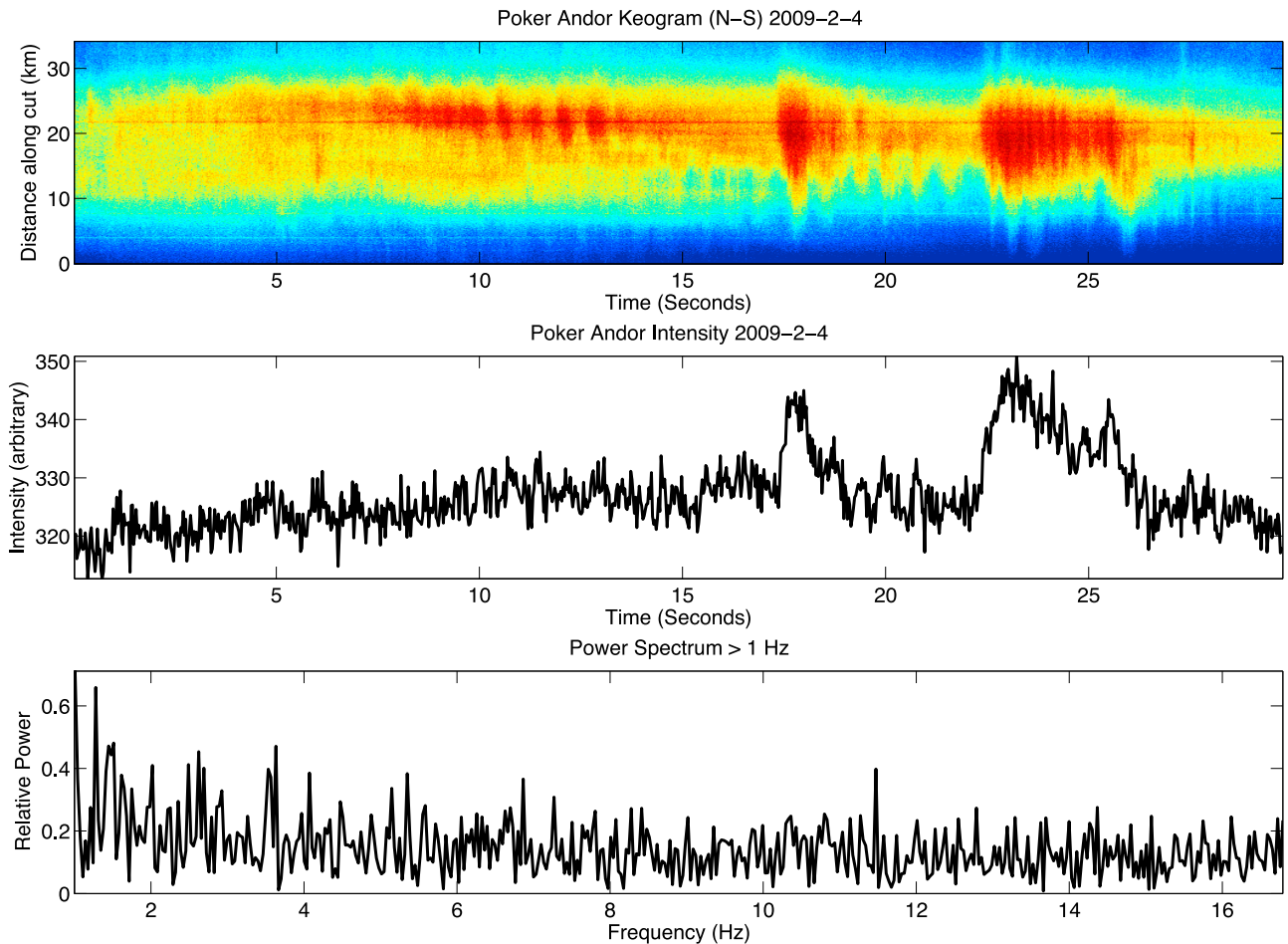


Figure 7. (top) Keogram along the North–South direction, through the center of the EMCCD narrowfield images, taken near 1110 UT. North is up and the horizontal lines are stars. (middle) Intensity profile taken along the center of the keogram. (bottom) FFT of the intensity cut.

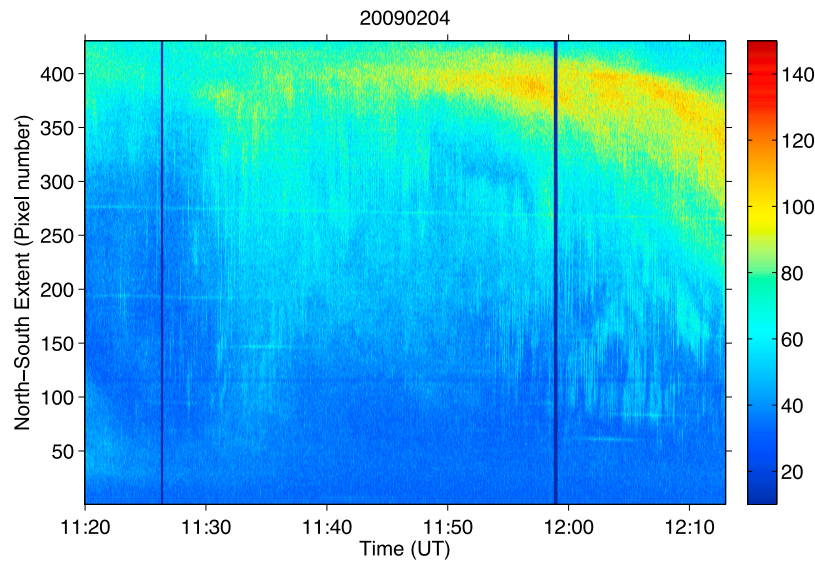


Figure 8. Keogram along the North–South direction, through the all-sky images for the time period 1120–1215 UT. North is up, the horizontal lines are stars, and the dark vertical lines are data gaps.

energy range (few keV to tens of keV) to produce diffuse aurora.

[26] An additional connection between the pulsating auroral structures and chorus waves can be made by examining recent modeling efforts. *Su et al.* [2009] investigated the evolution of electron pancake distributions [*Meredith et al.*, 1999, 2000] after substorm injections and the effects of chorus in resonant scattering of plasma sheet electrons. They concluded that lower band chorus can resonantly scatter ≥ 1 keV electrons into the loss cone and that the combined scattering of both upper and lower band chorus can cause rapid precipitation of keV electrons, resulting in diffuse aurora. The pulsating auroral observations presented show temporal development after the substorm injection,

with the most intense activity occurring several hours later. This is consistent with *Su et al.* [2009], where they found that the electron pancake distribution develops over time-scales of a few hours and can result in effectively scattering the electrons responsible for diffuse aurora into the loss cone.

[27] Table 1 presents a quantified comparison between the general characteristics of chorus elements and the features of the pulsating auroral structures presented here. The luminosity enhancements associated with the pulsating aurora closely match the characteristics of chorus elements, suggesting that some of these auroral features were likely caused by electrons that were scattered into the loss cone by specific chorus elements. A particularly interesting com-

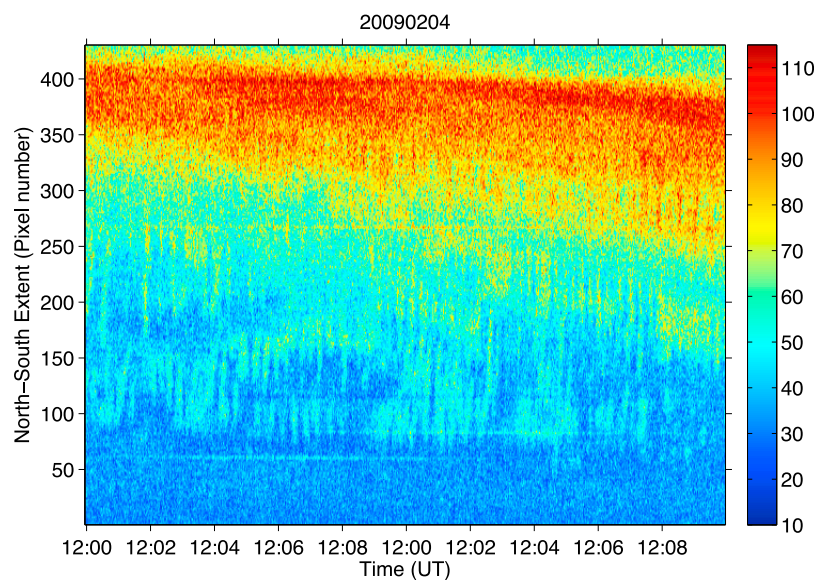


Figure 9. Ten minute section (1200–1210 UT) of the keogram in Figure 8, presented in the same format.

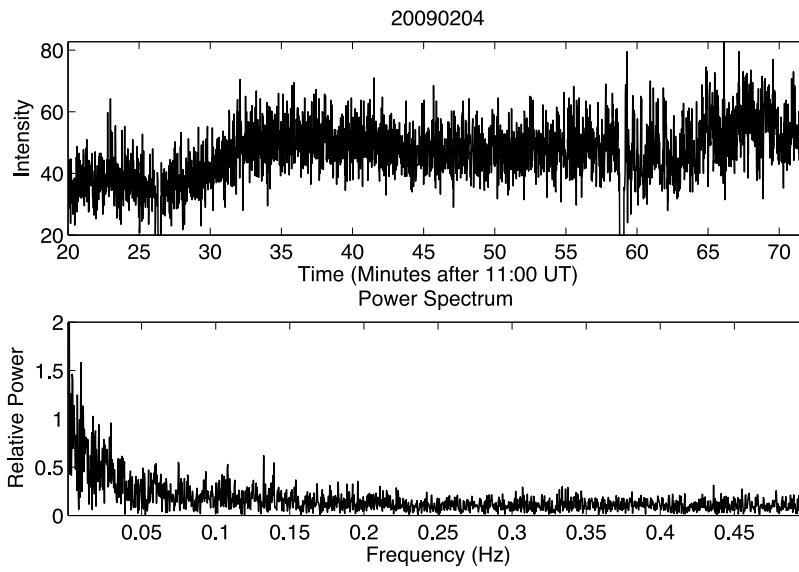


Figure 10. (top) Intensity as a function of time near the magnetic zenith (along pixel number 200 of Figure 8) from the all-sky imager data. (bottom) FFT of the intensity profile.

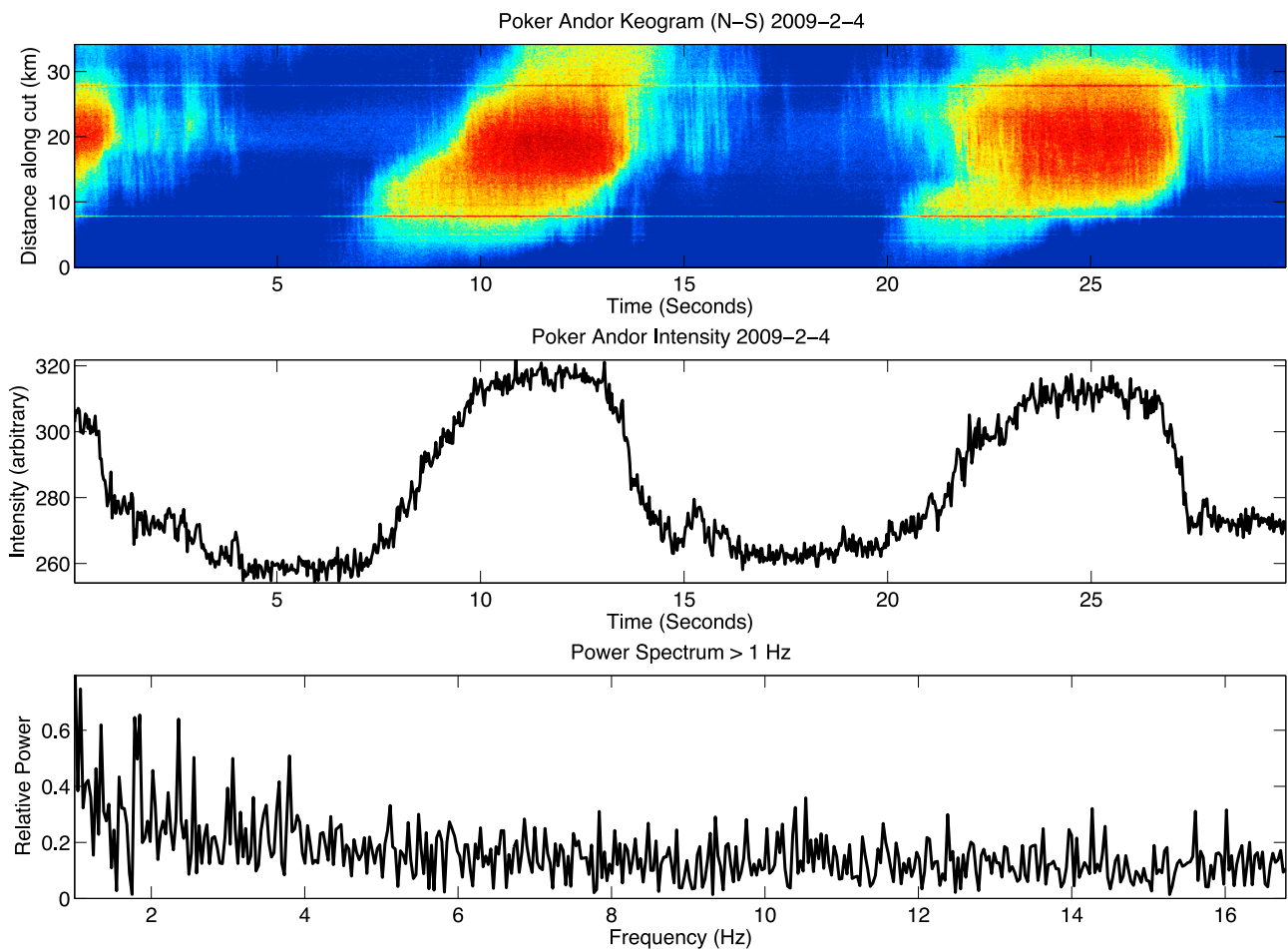


Figure 11. (top) Keogram along the North–South direction, through the center of the EMCCD narrowfield images, taken near 1205 UT. North is up and the horizontal lines are stars. (middle) Intensity profile taken along the center of the keogram. (bottom) FFT of the intensity cut.

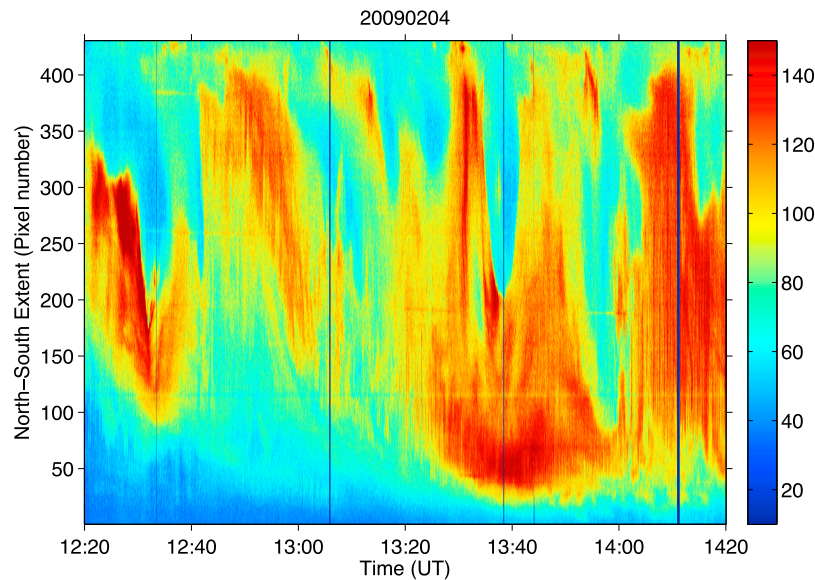


Figure 12. Keogram along the North–South direction, through the all-sky images for the time period 1220–1420 UT. North is up in, the horizontal lines are stars, and the dark vertical lines are data gaps.

parison can be made between Figure 7 (top), where there is an increase in the frequency of the pulsating inside the localized brightening of the aurora and Figure 3c of *Nunn et al.* [2009], where there is similarly an increase in the frequency of the upper band chorus element spacing inside the region where there is a localized grouping of lower band chorus elements. Figure 7 (top) and Figure 3c of *Nunn et al.* [2009] show striking similarity, despite being created by different means, suggesting a causal relationship between chorus elements and the luminosity enhancements of pulsating aurora. Furthermore, the modeling work of *Nunn et al.* [2009] showed that the resonant electron energy varied with the chorus element spacing, with closer spacing corresponding to higher energy

electrons. This offers a possible explanation as to why the higher frequency pulsations are associated with brighter aurora, since intensity is proportional to electron energy flux [*Stenbaek-Nielsen et al.*, 1998].

[28] The large scale structure and evolution of the pulsating auroral features revealed in the all-sky imager data, are consistent with chorus wave scattering in addition to ULF wave modulations. During the first period (1050–1120 UT), the diffuse aurora was moderately intense and moved South. The main frequency range that contained most of the power was ≤ 100 mHz. During the second period (1120–1215 UT), the aurora was mostly in the North and weaker. In this case the power was largely confined to fre-

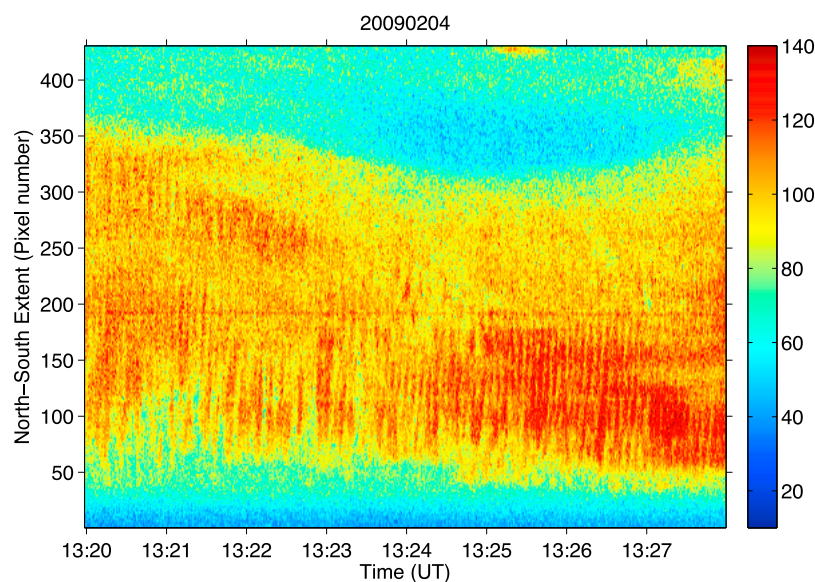


Figure 13. Eight minute section (1320–1328 UT) of the keogram in Figure 12, presented in the same format.

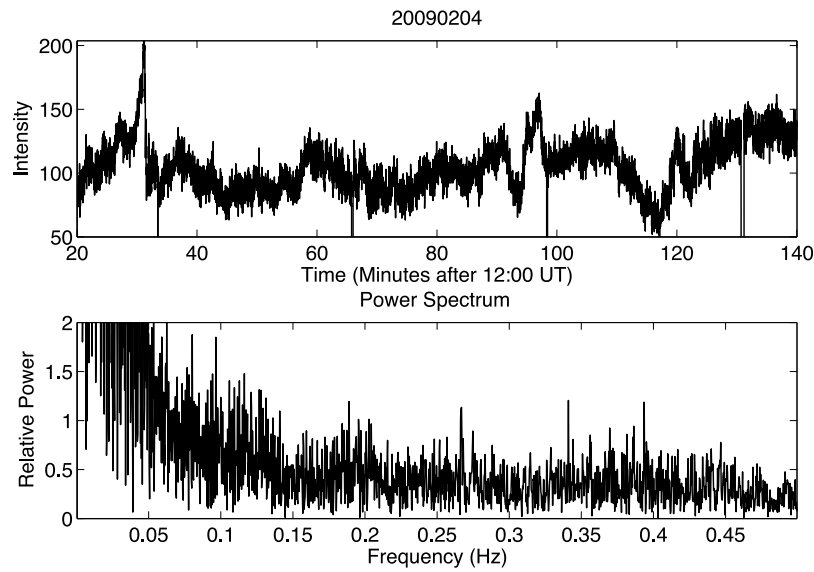


Figure 14. (top) Intensity as a function of time near the magnetic zenith (along pixel number 200 of Figure 12) from the all-sky imager data. (bottom) FFT of the intensity profile.

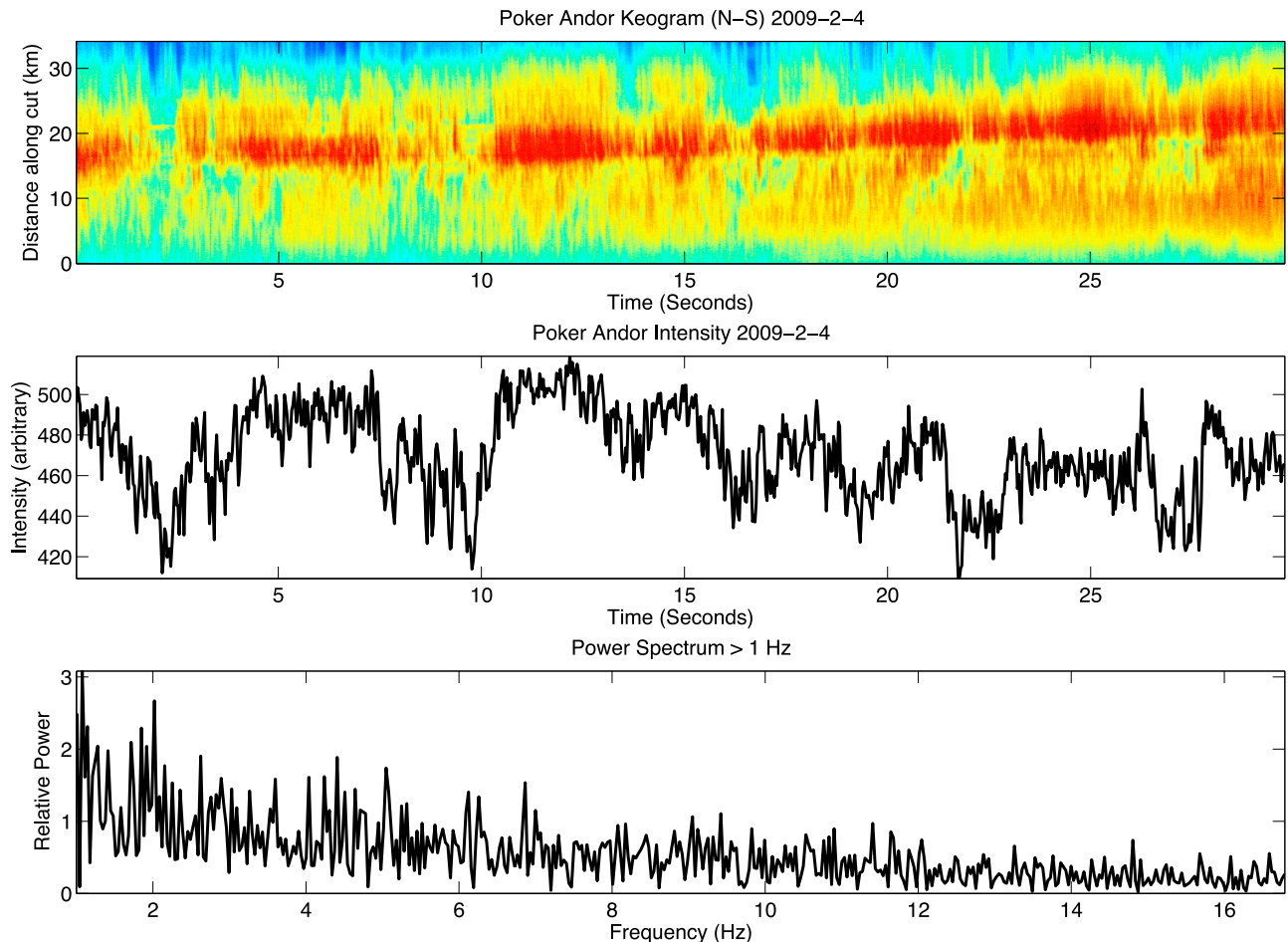


Figure 15. (top) Keogram along the North–South direction, through the center of the EMCCD narrow-field images, taken near 1325 UT. North is up and the horizontal lines are stars. (middle) Intensity profile taken along the center of the keogram. (bottom) FFT of the intensity cut.

Table 1. Comparison Between Observed Features of Chorus Emissions and the Characteristics of the Pulsating Aurora Luminosity Enhancements Presented in This Work

Feature	Chorus	Pulsating Aurora
Element spacing	0.1 to 5 s	0.1 to 1 s
Element duration	0.1 to 5 s	0.1 to 1 s
Grouping of elements	1 to 10 s	3 to 15 s
Local time	Midnight to morning sector	Midnight to morning sector
L-value	~4 to 11	~5 to 6

quencies ≤ 50 mHz. During the third period (1220–1420 UT), the aurora intensified significantly and moved further South. In the latter case the power was contained in the frequencies ≤ 150 mHz.

[29] One possible explanation for the change in frequency with time, is the change in length of the closed magnetic field line connected to Poker Flat. When the magnetosphere is compressed, the local L-value, and subsequently the field line length, is reduced resulting in higher frequency ULF waves. Hence, the change in frequency with the location of the aurora is possibly due to a change in the length of the magnetic field line at Poker Flat, which is consistent with the data for this case study. The causal relationship between ULF and chorus is not clear based on these data and therefore, additional events, and ideally simultaneous in situ measurements, are needed to fully test these hypotheses.

[30] The frequencies observed in each of the three time periods are summarized in Table 2. The first column contains the low frequencies, in mHz, from the all-sky imager data and the second the high frequencies, in Hz, from the narrowfield imager data. The frequency listed in parenthesis indicates the cutoff at which the power begins to significantly increase toward lower frequencies.

[31] There is a wide range of frequencies observed within the aurora, evidenced by the above FFT analysis summarized in Table 2. The frequencies present do not stay constant in time and the aurora does not remain stationary, suggesting that the specific frequencies measured actually depend on where and when it is measured. This indicates that there is likely a continuum of frequencies within the pulsating auroral structures.

[32] The discrete FFT analysis presented above is used for extracting specific frequencies at one location but does not account for the spatial variation of auroral structures. The high quality of the EMCCD narrowfield images allows for FFTs to be taken in the spatial dimensions as well. With both spatial and temporal FFTs, the creation of ω -k diagrams becomes possible. Figure 16 shows the ω -k diagrams for the three EMCCD narrowfield examples presented above. Figure 16 (top) is for the 1110 UT example, Figure 16 (middle) is for the 1205 UT example and Figure 16 (bottom) is for the 1325 UT example. Each one is created from 1000 images covering a 30 second time period. The y-axes are frequency in Hz and the x-axes are wave number in m^{-1} . All three are plotted on the same axes and intensity scales for comparison.

[33] This shows that the temporal frequencies are fairly continuous over the range in which they occur. In addition, there appears to be a continuous range of associated spatial scales. An interesting observation is that there is a pro-

gression of power to higher frequencies and smaller spatial scales over the course of the three hour time period.

4. Conclusions

[34] The luminosity variations of diffuse auroral structures can be used to investigate the magnetospheric wave processes responsible for scattering electrons into the loss cone. The 04 February 2009 event studied here contained a sub-storm followed by several hours of pulsating diffuse auroral structures. The data were examined in three distinct periods (1050–1120 UT, 1120–1215 UT, and 1220–1420 UT), based on PFISR electron density data.

[35] The pulsating structures and frequencies are consistent with the hypothesis that the electrons are coming from the plasma sheet by way of pitch angle scattering from chorus emissions, with the pulsating features corresponding to the discrete chorus elements.

[36] It is generally assumed that pulsating aurora is caused by resonantly scattered plasma sheet electrons and it is known to occur with frequencies in the few to few hundred mHz range. These frequencies are easily observable with all-sky imagers and can be detected even with a low cadence of one frame per second. However, the detection of higher frequencies (1 to 15 Hz) requires the use of narrow FOV imagers with fast frame rates of 30 frames per second or higher. This study used both types of imagers and found that the frequencies observed with the all-sky were consistent with what was expected. The narrowfield imager data revealed that many higher frequency pulsations (up to 12 Hz) were present at the same time as the low frequency ones. The frequencies observed with both imagers are summarized in Table 2. The wide range of frequencies observed together with the ω -k diagrams presented in Figure 16 indicate that there is likely a continuum of temporal and spatial frequencies present in the pulsating structures.

[37] There are three significant observations regarding the frequency of the pulsations and the occurrence of auroral structures, that can be made regarding this case study. The first is that brighter aurora tends to be associated with higher frequency pulsations. This is evident in both the low frequencies (from the all-sky data) and the high frequencies (from the narrowfield data). Moreover it is consistent with the modeling work of *Nunn et al.* [2009], that showed that closer chorus element spacing was associated with chorus waves resonating with higher energy electrons, increasing the net electron energy flux and in turn the auroral luminosity. Yet the possibility exists that the higher frequency pulsations are present at other times and thus an unrelated increase in energy flux allows them to be observed above

Table 2. Summary of the Frequency Ranges Containing Most of the Power Observed With the Two Different Imagers for Each distinct Time Period^a

Time Period	All-sky (mHz)	Narrowfield (Hz)
1 (1050–1120 UT)	≤ 100	≤ 8
2 (1120–1215 UT)	≤ 50	≤ 6
3 (1220–1420 UT)	≤ 150	≤ 12

^aThe all-sky imager column describes the low frequencies in mHz, while the narrowfield imager column describes the high frequencies in Hz.

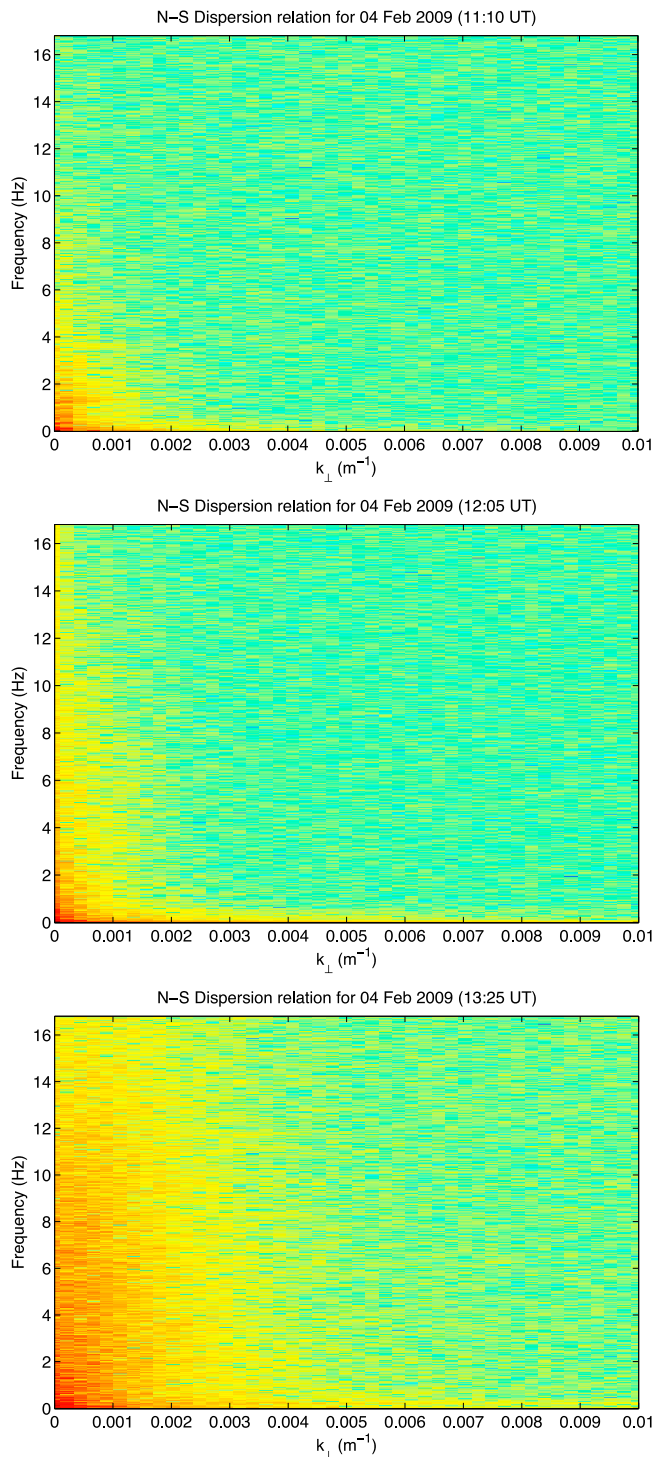


Figure 16. Shown are ω - k diagrams for the three EMCCD narrowfield data examples. The y axis is frequency in Hz, and the x axis is wave number in m^{-1} . All three are plotted on the same axes and intensity scales for comparison.

the noise floor. This, however, seems unlikely given the similar features observed in the chorus elements shown by Nunn *et al.* [2009]. The power in the low frequencies also increases in these regions, which is consistent with an overall increase in the scattering efficiency of the waves. The second significant observation is that the frequency of pulsation

appears to be inversely correlated with the horizontal width of the auroral fine structures, smaller structures are associated with faster frequencies. The ω - k diagrams indicate that higher temporal frequencies exist when there are smaller scale structures present, but a direct connection can not be established from these data alone. Last, the intensity of the aurora was not symmetric in time, around the pulsating patch. It appears to be a common feature of pulsating patches, where the intensity increases at a slower rate than it decreases. This could be the result of a time dispersion effect, where the higher energy electrons arrive first followed by a greater flux of lower energy electrons, where the steep decrease in luminosity corresponds to the emptying of the loss cone.

[38] The next step in comparing optical signatures to chorus waves is to develop a statistical picture of the occurrence of specific frequencies by examining many different events. In addition, in situ comparisons with conjugate ground-based optical observations, are now possible with the Themis constellation of satellites.

[39] **Acknowledgments.** This work was supported by National Science Foundation grant ATM-0836410. The authors would like to thank the University of Alaska, Fairbanks/Geophysical Institute for the use of their facilities and imagers at Poker Flat, Alaska, particularly H. C. Stenbaek-Nielsen and D. Hampton. We also thank SRI International and the entire PFISR crew for their support in coordinating the radar operations and obtaining the data.

[40] Robert Lysak thanks Ingrid Sandahl, Larry Lyons and another reviewer for their assistance in evaluating this paper.

References

- Belmont, G., D. Fontaine, and P. Canu (1983), Are equatorial electron cyclotron waves responsible for diffuse auroral electron precipitation?, *J. Geophys. Res.*, *88*, 9163–9170, doi:10.1029/JA088iA11p09163.
- Breneman, A. W., C. A. Kletzing, J. Pickett, J. Chum, and O. Santolik (2009), Statistics of multispacecraft observations of chorus dispersion and source location, *J. Geophys. Res.*, *114*, A06202, doi:10.1029/2008JA013549.
- Degeling, A. W., L. G. Ozeke, R. Rankin, I. R. Mann, and K. Kabin (2008), Drift resonant generation of peaked relativistic electron distributions by Pc 5 ULF waves, *J. Geophys. Res.*, *113*, A02208, doi:10.1029/2007JA012411.
- Kennel, C. F., F. L. Scarf, R. W. Fredricks, J. H. McGehee, and F. V. Coroniti (1970), VLF Electric Field Observations in the Magnetosphere, *J. Geophys. Res.*, *75*, 6136–6152, doi:10.1029/JA075i031p06136.
- Kokubun, S., K. Hayashi, T. Oguti, K. Tsuruda, S. Machida, T. Kitamura, O. Saka, and T. Watanabe (1981), Correlations between very low frequency chorus bursts and impulsive magnetic variations at $L = 4.5$, *Can. J. Phys.*, *59*, 1034–1041.
- Liang, J., W. W. Liu, E. F. Donovan, and E. Spanswick (2009), In-situ observation of ULF wave activities associated with substorm expansion phase onset and current disruption, *Ann. Geophys.*, *27*, 2191–2204.
- Lyons, L. R. (1974), Electron diffusion driven by magnetospheric electrostatic waves, *J. Geophys. Res.*, *79*, 575–580, doi:10.1029/JA079i004p00575.
- Meredith, N. P., A. D. Johnstone, S. Szita, R. B. Horne, and R. R. Anderson (1999), “Pancake” electron distributions in the outer radiation belts, *J. Geophys. Res.*, *104*, 12,431–12,444, doi:10.1029/1998JA900083.
- Meredith, N. P., R. B. Horne, A. D. Johnstone, and R. R. Anderson (2000), The temporal evolution of electron distributions and associated wave activity following substorm injections in the inner magnetosphere, *J. Geophys. Res.*, *105*, 12,907–12,917, doi:10.1029/2000JA900010.
- Meredith, N. P., R. B. Horne, R. M. Thorne, and R. R. Anderson (2009), Survey of upper band chorus and ECH waves: Implications for the diffuse aurora, *J. Geophys. Res.*, *114*, A07218, doi:10.1029/2009JA014230.
- Ni, B., R. M. Thorne, Y. Y. Shprits, and J. Bortnik (2008), Resonant scattering of plasma sheet electrons by whistler-mode chorus: Contribution to diffuse auroral precipitation, *Geophys. Res. Lett.*, *35*, L11106, doi:10.1029/2008GL034032.

- Nunn, D., O. Santolik, M. Rycroft, and V. Trakhtengerts (2009), On the numerical modelling of VLF chorus dynamical spectra, *Ann. Geophys.*, *27*, 2341–2359.
- O'Brien, T. P., K. R. Lorentzen, I. R. Mann, N. P. Meredith, J. B. Blake, J. F. Fennell, M. D. Looper, D. K. Milling, and R. R. Anderson (2003), Energization of relativistic electrons in the presence of ULF power and MeV microbursts: Evidence for dual ULF and VLF acceleration, *J. Geophys. Res.*, *108*(A8), 1329, doi:10.1029/2002JA009784.
- Peticolas, L. M., T. J. Hallinan, H. C. Stenbaek-Nielsen, J. W. Bonnell, and C. W. Carlson (2002), A study of black aurora from aircraft-based optical observations and plasma measurements on FAST, *J. Geophys. Res.*, *107*(A8), 1217, doi:10.1029/2001JA900157.
- Sergienko, T., I. Sandahl, B. Gustavsson, L. Andersson, U. Brändström, and Å. Steen (2008), A study of fine structure of diffuse aurora with ALIS-FAST measurements, *Ann. Geophys.*, *26*, 3185–3195.
- Skoug, R. M., S. Datta, M. P. McCarthy, and G. K. Parks (1996), A cyclotron resonance model of VLF chorus emissions detected during electron microburst precipitation, *J. Geophys. Res.*, *101*, 21,481–21,492, doi:10.1029/96JA02007.
- Stenbaek-Nielsen, H. C., T. J. Hallinan, D. L. Osborne, J. Kimball, C. Chaston, J. McFadden, G. Delory, M. Temerin, and C. W. Carlson (1998), Aircraft observations conjugate to FAST: Auroral arc thicknesses, *Geophys. Res. Lett.*, *25*, 2073–2076.
- Su, Z., H. Zheng, and S. Wang (2009), Evolution of electron pitch angle distribution due to interactions with whistler mode chorus following substorm injections, *J. Geophys. Res.*, *114*, A08202, doi:10.1029/2009JA014269.
- Trakhtengerts, V. Y. (1999), A generation mechanism for chorus emission, *Ann. Geophys.*, *17*, 95–100, doi:10.1007/s005850050739.
- Zolotukhina, N. A., P. N. Mager, and D. Y. Klimushkin (2008), Pc5 waves generated by substorm injection: A case study, *Ann. Geophys.*, *26*, 2053–2059.

M. Samara and R. G. Michell, Southwest Research Institute, 6220 Culebra Rd., San Antonio, TX 78238, USA. (msamara@swri.edu)